energies

MDPI

Article

Sliding Mode Self-Sensing Control of Synchronous Machine Using Super Twisting Interconnected Observers

Mohamed R. Kafi [1] , Mohamed A. Hamida [2], Hicham Chaoui [3,*] and Rabie Belkacemi [4]

[1]   Laboratoire de Génie Electrique, University Kasdi Merbah Ouargla, Ouargla 30000, Algeria;
      kafi.redouane@univ-ouargla.dz
[2]   Ecole Centrale de Nantes, LS2N UMR CNRS 6004, 44200 Nantes, France; mohamed.hamida@ec-nantes.fr
[3]   Intelligent Robotic and Energy Systems (IRES), Department of Electronics, Carleton University,
      1125 Colonel By Dr, Ottawa, ON K1S 5B6, Canada
[4]   Center for Energy Systems Research, Tennessee Technological University, Cookeville, TN 38505, USA;
      rbelkacemi@tntech.edu
*   Correspondence: hicham.chaoui@carleton.ca; Tel.: +1-613-520-2600; Fax: +1-613-520-5708

check for updates

Abstract: The aim of this study is to propose a self-sensing control of internal permanent-magnet synchronous machines (IPMSMs) based on new high order sliding mode approaches. The high order sliding mode control will be combined with the backstepping strategy to achieve global or semi global attraction and ensure finite time convergence. The proposed control strategy should be able to reject the unmatched perturbations and reject the external perturbation. On the other hand, the super-twisting algorithm will be combined with the interconnected observer methodology to propose the multi-input–multi-output observer. This observer will be used to estimate the rotor position, the rotor speed and the stator resistance. The proposed controller and observer ensure the finite-time convergence to the desired reference and measured state, respectively. The obtained results confirm the effectiveness of the suggested method in the presence of parametric uncertainties and unmeasured load torque at various speed ranges.

Keywords: self-sensing control; super twisting algorithm; synchronous machine; high order sliding mode; robust control; chattering phenomena

1. Introduction

Internal permanent-magnet synchronous machines (IPMSMs) have been getting progressively more popular in several industrial applications owing to high efficiency, good power density and finally the high torque/current ratio [1,2]. Despite its advantages, high-speed control remains a very significant and challenging subject of research [3,4], and the feedback information on rotor position remains of paramount importance. It is noticed that the utilization of encoders has many shortcomings, like decreased reliability of the system and the cost. As a result, self-sensing control has become attractive in many industrial applications.

To perform self-sensing control operations, various methods, like the one which uses the back electromotive force to control the IPMSM [5], have been proposed in the literature. This method offers a good performance at medium and high speeds [6]; however, it does not function at zero and very low speeds because of the integrator's drift problem, particularly in the analog realization. Moreover, this method is very sensitive to the variations of the stator resistance during operation. Alternatively, an extended electromotive force based method is suggested [7]. Moreover, to evaluate the speed and the related rotor's position, several observer-based methods are introduced in the

literature. An extended state observer is employed by [8]. The obtained results are convincing, with nominal motor parameters, but once the robustness tests are considered, the performance of this observer is degrading. To deal with this problem, an adaptive observer considers the electrical motor parameters [9]. This observer gives good results even with uncertain parameters but the developed algorithm is complicated and needs a lot of computing time [10]. A classical high gain observer is used in [11] to estimate the rotor speed and position. This observer is a good candidate to compensate the non-modelled dynamics; however, it is very sensitive to the measurement noises. To deal with this limitation, an adaptive version of this observer has been recently employed for self-sensing control of the induction machine [12]. Thanks to their robustness, the sliding mode observers are frequently used for speed and position estimation of electrical motors [13]. However, these observers suffer from the problem of chattering due to the high frequency commutation of the sign function [14]. To deal with this problem, higher order sliding mode observers are introduced. The super-twisting algorithm [15] is one of the most promising higher order sliding mode observers. The super-twisting algorithm is introduced in [15] for signal-input–signal-output systems. For the same objective, Kalman filter [16] has been developed. The filter which comprises prediction demands a large number of recursive calculations. However, it seems very challenging to ensure the convergence of the rotor's speed and position by the adoption of system control which is based on EKF.

Because of its simplicity, the method of flux linkage estimation is widely used [17]. This method has a disadvantage at low speed due to the serious problem of drift [18].

Non-model based approaches are also used for self-sensing control such as high-frequency injection [19,20] and artificial intelligence methods [21]. Degradation of the system performance can occur by high frequency injection due to the generated noise of the same nature [22].

The quasi-continuous HOSM, which is rather a combination of both an HOSM control and the backstepping approach control, is considered to trim down the chattering phenomenon effect [23]. This method is used for surface-mounted PMSM self-sensing control. The quasi-continuous HOSM controller does not take into consideration the perturbations which do not match. This invited the application of a new algorithm by a controller, which takes, however, into consideration the unmatched perturbations in case of self-sensing IPMSM. In [18], the authors propose a backstepping method whereby the electric current i_d is squeezed to zero. However, this method does not make a profit of the reluctance torque. In this work and to enhance the effectiveness of the IPMSM control, a maximum-torque per-ampere (MTPA) strategy is developed. In another aspect, the estimation of rotor position and velocity through a conventional observer based on the sliding mode approach was recommended in [24]; this has a higher precision estimation capability and better dynamic behavior. The chattering phenomena remains the major disadvantage of the conventional sliding mode observer due to discontinuous functions [25,26]. To decrease, therefore, the chattering phenomenon and to create an HOSM observer, a novel result [23] is employed. The applied results, thereafter, estimate, in a finite time, both the position and speed of the rotor, as well as the stator resistances that are known to be time-varying.

In this work, the main contribution is to develop a nonlinear controller with observer to control IPMSM without sensors.

This paper suggests a control scheme coupling two separate design methods, HOSM and backstepping control. To achieve a global or semi-global attraction domain, maintaining the finite-time exact tracking. With this algorithm, despite the presence of unmatched perturbations, i.e., parameter uncertainties and external disturbances, an exact finite-time tracking of the desired output is achieved. The desired dynamics for each state are determined by the previous state, and so forth until the first state, which is defined by the required tracking signal. Each virtual control consists of two parts, while the nominal portion of the system is compensated by the first part, the achievement of the desired dynamics despite the perturbations is concerned in second part.

The control strategies guarantee finite time precise pursuit of the desired output under MTPA operation and with the existence of unmatched perturbation. The combination of both the super

twisting algorithm and the interconnected technique provides a novel MIMO high order sliding observer. The suggested observer is to estimate both the rotor's position and speed at the different speed rate. In addition, the resistance of the rotor is estimated, which leads to better accuracy when the operating conditions change. The closed-loop system stability is provided by means of utilizing the nonlinear separation principles theorem, rather than several proposed self-sensing control methods for IPMSM.

2. Problem Statement

The IPMSM is usually modeled in the rotor synchronous rotating frame as [27]:

$$\begin{aligned}\dot{x} &= F(x) + G(x)u \\ y &= H(x)\end{aligned} \tag{1}$$

with $x = [i_d, i_q, \Omega, \theta]$, $u = [u_d, u_q]$, $y = [h_1, h_2] = [i_d, i_q]$

$$F(x) = \begin{bmatrix} -\frac{R_s}{L_d}i_d + p\frac{L_q}{L_d}\Omega i_q \\ -\frac{R_s}{L_q}i_q - p\frac{L_d}{L_q}\Omega i_d - p\frac{1}{L_q}\phi_f\Omega \\ \frac{p}{J}(L_d - L_q)i_d i_q - \frac{f_v}{J}\Omega + \frac{p}{J}\phi_f i_q - \frac{1}{J}T_l \\ \Omega \end{bmatrix},$$

$$g_1(x) = [\frac{1}{L_d} \quad 0 \quad 0 \quad 0], \quad g_2(x) = [0 \quad \frac{1}{L_q} \quad 0 \quad 0].$$

where i_d and i_q are stator currents, Ω and θ are the rotor mechanical speed and angular position, respectively, u_d and u_q are the stator voltages, R_s is the stator resistance, L_d and L_q are the dq-axis inductances, p is the number of pole pairs, Φ_f is permanent-magnet flux linkage, J is the moment of inertia, T_l is the load torque, and f_v is the viscous friction coefficient.

Remark 1. *The operating interval of IPMSM $\mathcal{D}_{om}$ is delimited by the values defined as follows:*

$$\mathcal{D}_{om} = \{X \in R^5 | \ |i_d| \le I_d^{max}, \ |i_q| \le I_q^{max}, \ |\Omega| \le \Omega^{max}, \ |R_s| \le R_s^{max}, \ |T_l| \le T_l^{max}\}$$

where $X = (\ i_d \ i_q \ \Omega \ R_s \ )^T$, and the present maximum values are, respectively, I_d^{max}, I_q^{max} for currents, Ω^{max} for speed, R_s^{max} for stator resistance and T_l^{max} for load torque; the values are defined in specification sheet from the motor's manufacturing.

Control objective: The main control design objective is to track the desired reference (Ω^*) for speed and following the desired trajectory for i_d^* despite uncertainties of parameters and disturbance in torque load.

Observation objective: The aim is to reconstruct the value of the IPMSM's speed, position, and stator resistance, by unique measurement of currents and voltages.

3. MTPA QC HOSM Control

The developed approach, as well as the application of IPMSM, will be detailed in the following section, starting by the QC HOSM method basics.

3.1. Quasi-Continuous Higher Order Sliding Mode Controller

In this section a solution for the control problem described in previous section is proposed. This solution combines the backstepping and higher order sliding mode methodologies as recommended by [28]. Consider the following nonlinear system:

$$
\Sigma : \begin{cases}
\dot{x}_1 &= f_1(x_1,t) + g_1(x_1,t)x_2 + \omega_1(x_1,t) \\
\dot{x}_i &= f_i(\overline{x}_i,t) + g_i(\overline{x}_i,t)x_{i+1} + \omega_i(\overline{x}_i,t) \\
\dot{x}_n &= f_n(x,t) + g_n(x,t)u + \omega_n(x,t) \\
y &= x_1
\end{cases}
\tag{2}
$$

where i varies from 2 to $(n-1)$, the state $x \in R^n$, with $x_i \in R$, $\overline{x}_i = [x_1, \ldots, x_i]^T$, and the control input is $u \in R$. In addition, $f_i(\overline{x}_i,t)$ and $g_i(\overline{x}_i,t)$ are the smooth function, the bounded unknown disturbance term $\omega_i(\overline{x}_i,t)$, representing the parameter variations, [29] as well as the external perturbations, admitting $n-i$ bounded derivatives at least.

$g_i(\overline{x}_i,t) \neq 0$ for $x \in X \subset R^n$, $t \in [0,\infty)$. For simplicity, suppose the relative degree of system (2) is n. For the nonlinear system class with unmatched disturbances (2), the control design procedure is presented as follows.

Step 1:

The first step consists to constructing the next virtual control $x_{i+1} = \phi_i$. For that, let us define $x_2 = \phi_1$ with ϕ_1 is $(n-1)$ times differentiable functions constructed as follows:

$$
\begin{aligned}
\phi_1 &= g_1(x_1,t)^{-1}\{f_1(x_1,t) + u_{1,1}\} \\
\dot{u}_{1,1} &= u_{1,2} \\
&\vdots \\
\dot{u}_{n,n-1} &= \lambda_1 \Psi_{n-1,n}\{\sigma_1, \dot{\sigma}_1, \ldots, \sigma_1^{n-1}\}
\end{aligned}
\tag{3}
$$

where $\sigma_1 = y - y_{ref}$. At the present stage, the virtual control consists of two parts ϕ_1 and $u_{1,1}$, respectively, providing compensation for the nominal part and, on the other hand, disturbances introduced by the $n-1$ integrators. The i-th step is as follows. The constructed virtual controller will be used in the next step as a reference in order to construct a new virtual control or a final control depending on the relative degree of the studied system.

Step i:

Considering the virtual control such that $x_{i+1} = \phi_i$, where ϕ_i is $n-i$ times the differentiable function given by:

$$
\begin{aligned}
\phi_i(\overline{x}_i,t,u_i) &= g_i(\overline{x}_i,t)^{-1}\{f_i(\overline{x}_i,t) + u_{i,1}\} \\
\dot{u}_{i,1} &= u_{i,2} \\
&\vdots \\
\dot{u}_{i,n-i} &= \lambda_i \Psi_{n-i,n-i+1}\{\sigma_i, \dot{\sigma}_i, \ldots, \sigma_i^{n-i}\}
\end{aligned}
\tag{4}
$$

where $\sigma_i = x_i - \phi_{i-1}$. Finally, the robust control law u is calculated at the last step.

Step n:

Taking $\sigma_n = x_n - \phi_{n-1}$, the actual effective control u is provided by

$$
\begin{aligned}
u &= g_n(x,t)^{-1}\{f_n(x,t) + u_{n,1}\} \\
u_{n,1} &= \lambda_n sign\{\sigma_n\}.
\end{aligned}
\tag{5}
$$

This controller ensures the finite-time convergence of the system states to their desired references despite the presence of the perturbations and parameter uncertainties.

In the following, this control strategy will be applied for the IPMSM case.

3.2. IPMSM Controller Design

In accordance with the control design procedure, a design of a quasi-continuous homogeneous control law for the synchronous motor is achieved, starting with the mathematical machine model (1), written as follows:

$$\Sigma_1 : \begin{cases} \dot{\Omega} &= \frac{p}{J}(L_d - L_q)i_d i_q + p\frac{\phi_f}{J}i_q - \frac{f_v}{J}\Omega - \frac{1}{J}T_l \\ \dot{i}_q &= -p\frac{\phi_f}{L_q}\Omega - p\frac{L_d}{L_q}\Omega i_d - \frac{R_s}{L_q}i_q + \frac{1}{L_q}u_q \end{cases} \tag{6}$$

$$\Sigma_2 : \begin{cases} \dot{i}_d &= -\frac{R_s}{L_d}i_d + p\frac{L_q}{L_d}\Omega i_q + \frac{1}{L_d}u_d \end{cases} \tag{7}$$

where $[x_{1,1}, x_{1,2}]^T := [\Omega, i_q]^T$ and $[x_{2,1}] := [i_d]$, $m = 2$. While the controlled outputs are $[\Omega, i_d]^T$, the relative degree of the vector is equal to $[2, 1]^T$. Models (6) and (7) are expressed as an interconnected system; in each term the subsystems are bounded and considered as external disturbances:

$$\Sigma_1 : \begin{cases} \dot{x}_{1,1} &= f_{1,1}(x_{1,1}) + g_{1,1}(x_{1,1})x_{1,2} + \omega_{1,1} \\ \dot{x}_{1,2} &= f_{1,2}(x_{1,2}) + g_{1,2}(x_{1,2})u_1 + \omega_{1,2} \end{cases} \tag{8}$$

$$\Sigma_2 : \begin{cases} \dot{x}_{2,1} &= f_{2,1}(x_{2,1}) + g_{2,1}(x_{2,1})u_2 + \omega_{2,1}. \end{cases} \tag{9}$$

with $\omega_{1,1}$, $\omega_{1,2}$, and $\omega_{2,1}$ being limited terms due, on the one hand, to the variable parameters and, on the other, to the terms of the connection, as well as to the external disturbances (namely, the load torque), where $f_{1,1}(x_{1,1}) = -\frac{f_v}{J}\Omega$, $g_{1,1}(x_{1,1}) = p\frac{\phi_f}{J}$, $\omega_{1,1} = \frac{p}{J}(L_d - L_q)i_d i_q - \frac{1}{J}T_l$, $f_{1,2}(x_{1,2}) = -\frac{R_s}{L_q}i_q$, $g_{1,2}(x_{1,2}) = \frac{1}{L_q}$ $\omega_{1,2} = -p\frac{\phi_f}{L_q}\Omega - p\frac{L_d}{L_q}\Omega i_d$. $f_{2,1}(x_{2,1}) = -\frac{R_s}{L_d}i_d$, $g_{2,1}(x_{2,1}) = \frac{1}{L_d}$ and $\omega_{2,1} = +p\frac{L_q}{L_d}\Omega i_q$.

Sliding surfaces are chosen that guarantee the trajectories are asymptotically stable during the sliding phase (see [28] for more details). The sliding surfaces chosen are proposed to realize the control objective by considering both model uncertainties and external disturbances.

Speed control loop

A homogeneous QC control is now applied to the speed loop. Consider the tracking error σ_Ω:

$$\sigma_\Omega = \sigma_{1,1} = \Omega - \Omega^*.$$

First stage

Define $x_{1,2} = \phi_{1,1}$; where $\phi_{1,1} = g_{1,1}(x_{1,1})^{-1}\{-f_{1,1}(x_{1,1}) + u_{(1,1)}\}$

Second stage

The virtual control $u_{1,1}$ can be written as:

$$\dot{u}_{(1,1)} = -\lambda_{1,1}\Psi_{(1,2)}(\sigma_{1,1}, \dot{\sigma}_{1,1})$$

$$\dot{u}_{(1,1)} = -\lambda_{1,1}\left\{\frac{\dot{\sigma}_{1,1} + |\sigma_{1,1}|^{\frac{1}{2}} sign(\sigma_{1,1})}{|\sigma_{1,1}|^{\frac{1}{2}} + |\dot{\sigma}_{1,1}|}\right\}.$$

after, the control action $u_q = u_1$ can be elaborated, considering:

$$\sigma_{1,2} = x_{1,2} - \phi_{1,1}.$$

Next, the first subsystem control can be written as

$$u_1 = g_{1,2}^{-1}(x_{1,2})\{-f_{1,2}(x_{1,2}) + u_{(1,2)}\}$$

where

$$u_{(1,2)} = -\lambda_{1,2} sign(\sigma_{1,2}).$$

Finally, we obtain

$$u_q = L_q \{ + \frac{R_s}{L_q} i_q + \lambda_{1,2} sign(i_q - \phi_{1,1}) \} \tag{10}$$

$\phi_{1,1} = \{ p \frac{\phi_f}{J} \}^{-1} \{ -\frac{f_v}{J} \Omega + u_{(1,1)} \}.$
Current i_d control loop.
Considering the IPMSM torque as follows:

$$T_e = p[\Phi_f i_q + (L_d - L_q) i_d i_q]. \tag{11}$$

the d-axis current has been subject to a control by forcing it to zero, which means $i_d^* = 0$. Yet the present approach does not make use of electromagnetic torque of an IPMSM. Despite considerable research on the current control of the axis d (i.e., $i_d^* = 0$), the electromagnetic torque of IPMSM remains inefficiently used. The Maximum-Torque-Per-Ampere control approach gives a highest torque/current proportion, wherefrom its effectiveness is improved [30]. Based on the MTPA control method below rated speed, the full use of the reluctance torque and the motor's operation with optimum performance determine the i_d^*. The process is achieved through the differentiation of Equation (11) maintaining the constancy of the current stators' absolute value i_d at the level of its highest value I_m as shown in [30]. The interconnection of the currents of the stator i_d & i_q, $i_d = f(i_q)$ can be written as:

$$i_d^* = -\frac{\Phi_f}{2(L_d - L_q)} - \sqrt{\frac{\Phi_f^2}{4(L_d - L_q)^2} + i_q^2}. \tag{12}$$

To implement the MTPA approach, the current i_d is pushed to go with the reference calculated in (12). Consider the next sliding surface

$$\sigma_{i_d} = \sigma_{2,1} = i_d - i_d^*.$$

Note that $r_2 = 1$. Then, the control effect for the second subsystem is written as

$$u_2 = g_{2,1}^{-1}(x_{2,1}) \{ -f_{2,1}(x_{2,1}) + u_{(2,1)} \} \tag{13}$$

where $u_{(2,1)} = -\lambda_{2,1} sign(\sigma_{2,1})$.
Finally, the controller is given by

$$u_d = L_d \{ \frac{R_s}{L_d} i_d + \lambda_{2,1} sign(i_d - i_d^*) \}. \tag{14}$$

4. Interconnected Observer Based HOSM Design for IPMSM

4.1. The Super Twisting Algorithm

Consider the next system

$$\begin{aligned} \dot{x}_1 &= x_2 \\ \dot{x}_2 &= f(t, x_1, x_2, u) + \zeta(t, x_1, x_2, u) \\ y &= x_1 \end{aligned} \tag{15}$$

The system (15) is resolved by forming it in the sense of Filippov ([31]). Supposing that the Lebesgue-measurable function $f(t, x_1, x_2, u)$ and the uncertainty function $\zeta(t, x_1, x_2, u)$ are uniformly

bounded in all compact regions of the state space (x_1, x_2), then the common form of the ST observer would be as follows

$$
\begin{aligned}
\dot{\hat{x}}_1 &= \hat{x}_2 + \alpha_1 |x_1 - \hat{x}_1|^{1/2} sign(x_1 - \hat{x}_1) \\
\dot{\hat{x}}_2 &= f(t, x_1, \hat{x}_2, u) + \zeta(t, x_1, \hat{x}_2, u) + \alpha_2 sign(x_1 - \hat{x}_1) \\
y &= x_1
\end{aligned}
\tag{16}
$$

Considering the estimated states as $\hat{x}_1$ and $\hat{x}_2$, and the observation gains as α_1, α_2.

4.2. HOSM Rotor Position Observer

To design a novel high order sliding mode observer, a combination of both the interconnected observer methodology and the super twisting method [23] is required. To evaluate the position and speed of the motor rotor as well as the stator resistance, an observer has been employed. The mathematical model of IPMSM within an $\alpha - \beta$ framework is written as:

$$
\begin{aligned}
\begin{pmatrix} \dot{i}_\alpha \\ \dot{i}_\beta \end{pmatrix} &= D^{-1} \left\{ \left(\begin{pmatrix} L_0 & 0 \\ 0 & L_0 \end{pmatrix} + \begin{pmatrix} A_{11} & A_{12} \\ A_{21} & A_{22} \end{pmatrix} \right) \right. \\
&\left. \left\{ - \begin{pmatrix} B_{11} & B_{12} \\ B_{21} & B_{22} \end{pmatrix} \begin{pmatrix} i_\alpha \\ i_\beta \end{pmatrix} + \begin{pmatrix} v_\alpha \\ v_\beta \end{pmatrix} - \omega\phi_f \begin{pmatrix} -\sin\theta_e \\ \cos\theta_e \end{pmatrix} \right\} \right\}
\end{aligned}
\tag{17}
$$

where

$A_{11} = -L_1 cos(2\theta_e)$, $A_{12} = -L_1 sin(2\theta_e)$, $A_{21} = -L_1 sin(2\theta_e)$, $A_{22} = +L_1 cos(2\theta_e)$,
$B_{11} = R_s - 2\omega L_{\alpha\beta}$, $B_{12} = 2\omega L_1 cos(2\theta_e)$, $B_{21} = 2\omega L_1 cos(2\theta_e)$, $B_{22} = R_s + 2\omega L_{\alpha\beta}$.

It is essential to reformulate the model in an appropriate expression, in order to design these observers. For this reason, the following change of coordinates is considered

$$
\begin{pmatrix} \xi_{11} \\ \xi_{12} \end{pmatrix} = \begin{pmatrix} i_\alpha \\ K_s sin(\theta_e)\omega \end{pmatrix} \quad \text{and} \quad \begin{pmatrix} \xi_{21} \\ \xi_{22} \end{pmatrix} = \begin{pmatrix} i_\beta \\ -K_s sin(\theta_e)\omega \end{pmatrix},
\tag{18}
$$

with $K_s = D^{-1}L_0\phi_f$, the system dynamics are:

$$
\Sigma_{\xi,i} : \begin{pmatrix} \dot{\xi}_{i1} \\ \dot{\xi}_{i2} \end{pmatrix} = \begin{pmatrix} 0 & 1 \\ 0 & 0 \end{pmatrix} \begin{pmatrix} \xi_{i1} \\ \xi_{i2} \end{pmatrix} + \begin{pmatrix} \Phi_i \\ F_i \end{pmatrix} + \begin{pmatrix} \Delta\zeta_{i1} \\ \Delta\zeta_{i2} \end{pmatrix}, i = 1.2;
\tag{19}
$$

where

$$
\begin{pmatrix} \Phi_1 \\ F_1 \end{pmatrix} = \begin{pmatrix} D^{-1}L_0 v_\alpha \\ -\frac{f_v}{J}\xi_{12} \end{pmatrix}, \quad \begin{pmatrix} \Phi_2 \\ F_2 \end{pmatrix} = \begin{pmatrix} D^{-1}L_0 v_\beta \\ -\frac{f_v}{J}\xi_{22} \end{pmatrix}
$$

with

$$
\begin{pmatrix} \Delta\zeta_{11} \\ \Delta\zeta_{12} \end{pmatrix}
$$

$$
= \begin{pmatrix} D^{-1}L_0(-B_{11}i_\alpha - B_{12}i_\beta) + D^{-1}(A_{11}(-B_{11}i_\alpha - B_{12}i_\beta + v_\alpha + \omega sin(\theta_e)) + \\ A_{12}(-B_{21}i_\alpha - B_{22}i_\beta + v_\beta - \omega cos(\theta_e))) \\ K_s cos(\theta_e)\omega^2 + K_s sin(\theta_e)(\frac{p}{J}[2L_1(cos(\theta_e i_\alpha + sin(\theta_e)\theta_e)i_\beta) + \phi_f][-sin(\theta_e)i_\alpha \\ + cos(\theta_e)i_\beta]) \end{pmatrix},
$$

and

$$
\begin{pmatrix} \Delta\zeta_{21} \\ \Delta\zeta_{22} \end{pmatrix} = \begin{pmatrix} D^{-1}L_0(-B_{21}i_\alpha - B_{22}i_\beta) + D^{-1}(A_{21}(-B_{11}i_\alpha - B_{12}i_\beta + v_\alpha + \omega sin(\theta_e)) + \\ A_{22}(-B_{21}i_\alpha - B_{22}i_\beta + v_\beta - \omega cos(\theta_e))) \\ K_s sin(\theta_e)\omega^2 - K_s cos(\theta_e)(\frac{p}{J}[2L_1(cos(\theta_e i_\alpha + sin(\theta_e)\theta_e)i_\beta) + \phi_f][-sin(\theta_e)i_\alpha \\ +cos(\theta_e)i_\beta]) \end{pmatrix}.
$$

Since the system (19) is currently in the appropriate form, it is feasible to conceive a finite-time observer for the MIMO system which is the SISO's extension as in [23].

Then, for the previous system (19), the design of an HOSM interconnected observer is performed:

$$
\hat{\Sigma}_{\xi,i} : \begin{pmatrix} \dot{\hat{\xi}}_{i1} \\ \dot{\hat{\xi}}_{i2} \end{pmatrix} = \begin{pmatrix} 0 & 1 \\ 0 & 0 \end{pmatrix} \begin{pmatrix} \hat{\xi}_{i1} \\ \hat{\xi}_{i2} \end{pmatrix} + \begin{pmatrix} \Phi_i \\ \hat{F}_i \end{pmatrix} + \begin{pmatrix} \lambda_{i1} |\tilde{\xi}_{i1}|^{1/2} sign(\tilde{\xi}_{i1}) \\ \lambda_{i2} sign(\tilde{\xi}_{i1}) \end{pmatrix}, i = 1, 2; \quad (20)
$$

where $(\hat{\xi}_{i1} \ \hat{\xi}_{i2})^T$ and $\tilde{\xi}_{i1} = \xi_{i1} - \hat{\xi}_{i1}$ are, respectively, the $\Sigma_{\xi,i}$ system's state estimation and the estimation error, for $i = 1, 2$; the rotor position estimation can be written, according to (20), as

$$
\hat{\theta}_e = tan^{-1}(\frac{\hat{\xi}_{12}}{\hat{\xi}_{22}}). \quad (21)
$$

Remark 2. *For the observer implementation, a four-quadrant inverse tangent (ATAN2 when using Matlab software) was used.*

4.3. Convergence of High-Order Sliding-Mode Observers

This section analyzes the convergence in finite time of the HOSM observer. The estimation of the error dynamics could be the following:

$$
\begin{pmatrix} \dot{\tilde{\xi}}_{i1} \\ \dot{\tilde{\xi}}_{i2} \end{pmatrix} = \begin{pmatrix} 0 & 1 \\ 0 & 0 \end{pmatrix} \begin{pmatrix} \tilde{\xi}_{i1} \\ \tilde{\xi}_{i2} \end{pmatrix} - \begin{pmatrix} \alpha_{i1} |\tilde{\xi}_{i1}|^{1/2} sign(\tilde{\xi}_{i1}) \\ \alpha_{i2} sign(\tilde{\xi}_{i1}) \end{pmatrix} + \begin{pmatrix} \Delta\zeta_{i1} \\ \tilde{F}_i(\hat{\xi}_1, \hat{\xi}_2) \end{pmatrix} \quad (22)
$$

where $\tilde{F}_i(\xi_{12}, \xi_{22}, \hat{\xi}_{12}, \hat{\xi}_{22}) = F_i(\xi_{12}, \xi_{22}) - \hat{F}_i(\hat{\xi}_{12}, \hat{\xi}_{22}) + \Delta\zeta_{i2}$.

With purpose of guaranteeing the existence of f_i as an upper bound, in practice, the states ξ_1 and ξ_2 are supposed to operate in a limited range within $\mathcal{D}_{om}$, [23], such that

$$
\left| \tilde{F}_i \right| = \left| F_i(\xi_{i1}, \xi_{i2}) - F_i(\xi_{i1}, \hat{\xi}_{i2}) + \Delta\zeta_{i2} \right| < \tilde{f}_i^+, \text{ for } i = 1, 2; \quad (23)
$$

holds for all ξ_1, ξ_2, in the domain $\mathcal{D}_{om}$, $\|\hat{\xi}_{i2}\| \leq 2 \sup \|\xi_{i2}\|$ is verified.

Assumption 1. *Assume there is an upper bound for the uncertainties $\Delta\zeta_{i1}$ and their corresponding derivative, such that:*

$$
\begin{cases} \|\Delta\zeta_{i1}\| < h_i, \text{ and} \\ \\ \left\| \frac{d\Delta\zeta_{i1}}{dt} \right\| < h_i' \end{cases} \quad \text{for} \quad i = 1, 2
$$

where h_i and h_i' are positive bounds.

Theorem 1. *Taking system (19), and admitting the verification of Assumption 1 and condition (23), in all operating ranges of $\mathcal{D}_{om}$, the initial conditions $\xi_{i1}(0), \xi_{i2}(0)$ and $\hat{\xi}_{i1}(0), \hat{\xi}_{i2}(0)$ are associated to observer gain α_{i1}, α_{i2} according to*

$$\begin{cases} \alpha_{i1} & > & \sqrt{\dfrac{2}{\alpha_{i2}+\tilde{f}_i^+}}\left(\dfrac{\alpha_{i2}-\tilde{f}_i^+-h_i'}{h_i'}\right), \\ \alpha_{i2} & > & \tilde{f}_i^+, \text{ for } i = 1,2, \end{cases} \tag{24}$$

The estimate state $\hat{\xi}_{i,j}$ converges in finite-time to the real states $\xi_{i,j}$, for $i,j = 1,2$, and there exists a time constant T_0 such that for all $T_0 \leq t$, $\hat{\xi}_{i,j} = \xi_{i,j}$, for $i,j = 1,2$.

4.4. Hosm Speed and Resistance Observer

Start by the observation that the behavior of resistance of the stator changes very slowly in a time lapse, which allows to model it by a piecewise function such that $\dot{R}_s = 0$, as a result of which the IPMSM (1) mathematical model can be decomposed into subsystems as follows.

$$\Sigma_{2.1}: \begin{cases} \dfrac{di_d}{dt} & = & -\dfrac{R_s}{L_d}i_d + p\dfrac{L_q}{L_d}\Omega i_q + \dfrac{1}{L_d}v_d \\ \dfrac{dR_s}{dt} & = & 0 \end{cases} \tag{25}$$

$$\Sigma_{2.2}: \begin{cases} \dfrac{di_q}{dt} & = & -\dfrac{R_s}{L_q}i_q - p\dfrac{L_d}{L_q}\Omega i_d - p\dfrac{1}{L_q}\phi_f\Omega + \dfrac{1}{L_q}v_q \\ \dfrac{d\Omega}{dt} & = & \dfrac{p}{J}(L_d - L_q)i_d i_q - \dfrac{f_v}{J}\Omega + \dfrac{p}{J}\phi_f i_q + \dfrac{T_l}{J}. \end{cases} \tag{26}$$

To write subsystems (25) and (26) so that the super-torque algorithm can be implemented, the following coordinate changes are considered:

$$\begin{pmatrix} \chi_{11} \\ \chi_{12} \end{pmatrix} = \begin{pmatrix} i_d \\ -R_s\frac{i_d}{L_d} \end{pmatrix} \quad \text{and} \quad \begin{pmatrix} \chi_{21} \\ \chi_{22} \end{pmatrix} = \begin{pmatrix} i_q \\ -p\Omega(\frac{\phi_f}{L_q} + \frac{L_d}{L_q}i_d) \end{pmatrix}, \tag{27}$$

Then, the representation of systems (25) and (26) can be written as:

$$\Sigma_{\chi,i} := \begin{pmatrix} \dot{\chi}_{i1} \\ \dot{\chi}_{i2} \end{pmatrix} = \begin{pmatrix} 0 & 1 \\ 0 & 0 \end{pmatrix}\begin{pmatrix} \chi_{i1} \\ \chi_{i2} \end{pmatrix} + \begin{pmatrix} \Gamma_i \\ H_i \end{pmatrix} + \begin{pmatrix} \Delta\rho_{i1} \\ \Delta\rho_{i2} \end{pmatrix} \tag{28}$$

where χ_{i1} and χ_{i2} for $i = 1,2$ are, respectively, the measured output and the unmeasured state that will be estimated, so T_l is taken into account as a limited bound disturbance because it is not measured. The terms Γ_i, H_i and ϕ_i for $i = 1,2$ can be written as:

$$\begin{pmatrix} \Gamma_1 \\ H_1 \end{pmatrix} = \begin{pmatrix} \frac{1}{L_d}v_d \\ (\frac{\chi_{12}}{\chi_{11}})^2 - \frac{\chi_{12}}{L_d\chi_{11}}v_d \end{pmatrix},$$

$$\begin{pmatrix} \Gamma_2 \\ H_2 \end{pmatrix} = \begin{pmatrix} \frac{1}{L_q}v_q \\ \{(-\frac{p^2}{J}(L_d-L_q)\chi_{11}\chi_{21} - \frac{F_v}{J}\frac{\chi_{22}}{\frac{\phi_f}{L_q}+\frac{L_d}{L_q}\chi_{11}} - \frac{p^2}{J}\phi_f\chi_{21}) \\ +(\frac{\phi_f}{L_d}+\frac{L_d}{L_q}\chi_{11}) + \frac{\chi_{22}}{\frac{\phi_f}{L_q}+\frac{L_d}{L_q}\chi_{11}}(-\frac{\chi_{22}\chi_{21}}{\frac{\phi_f}{L_q}+\frac{L_d}{L_q}\chi_{11}} + \frac{1}{L_q}v_d)\} \end{pmatrix}$$

$$\begin{pmatrix} \Delta\rho_{11} \\ \Delta\rho_{12} \end{pmatrix} = \begin{pmatrix} -\frac{L_d\chi_{22}\chi_{12}}{\Phi_f+L_d\chi_{11}} \\ -\frac{\chi_{12}\chi_{22}\chi_{21}}{L_d\chi_{11}(\Phi_f+L_d\chi_{11})} \end{pmatrix}, \quad \begin{pmatrix} \Delta\rho_{21} \\ \Delta\rho_{22} \end{pmatrix} = \begin{pmatrix} -\frac{L_d\chi_{12}\chi_{21}}{L_q\chi_{11}} \\ \frac{L_d\chi_{12}\chi_{22}}{\Phi_f+L_d\chi_{11}} + \frac{T_l}{J} \end{pmatrix}.$$

where $\Delta\rho_{ij}$ for $i,j = 1,2$; are the interrelated terms. These terms are thought of as disturbances.

Based on the extension of [23], an interrelated second-order sliding mode (ISOSM) observer for subsystems (25) and (26) is designed as follows. The HOSM interconnected observer for systems (25) and (26) is considered as

$$\widehat{\Sigma}_{\chi,i} := \begin{pmatrix} \dot{\hat{\chi}}_{i1} \\ \dot{\hat{\chi}}_{i2} \end{pmatrix} = \begin{pmatrix} 0 & 1 \\ 0 & 0 \end{pmatrix} \begin{pmatrix} \hat{\chi}_{i1} \\ \hat{\chi}_{i2} \end{pmatrix} + \begin{pmatrix} \Gamma_i \\ \hat{H}_i \end{pmatrix} + \begin{pmatrix} \alpha_{i1} |\tilde{\chi}_{i1}|^{1/2} sign(\tilde{\chi}_{i1}) \\ \alpha_{i2} sign(\tilde{\chi}_{i1}) \end{pmatrix} \qquad (29)$$

where $\tilde{\chi}_{i1} = \chi_{i1} - \hat{\chi}_{i1}$, for $i = 1, 2$, where $(\hat{\chi}_{i1} \ \hat{\chi}_{i2})^T$ is $\Sigma_{\chi,i}$ system state estimation.

By considering (27), the resistance and speed estimation of the stator is given by:

$$\hat{R}_s = -\frac{L_d \hat{\chi}_{12}}{\hat{\chi}_{11}}, \qquad \Omega = -\frac{L_q \hat{\chi}_{22}}{p(\Phi_f + L_d \hat{\chi}_{11})} \qquad (30)$$

Remark 3. *In the same way as that adopted in Section 4.3, the convergence of observers (29) can be proved.*

Remark 4. *Separation principle. Presented in [4,23], the principle of separation is achieved by consolidating the observer once its temporal convergence is limited, and consolidating a controller.*

The controller will still not be applied in the first time interval from 0 to T, while, at this time, the state estimation converges to the state of the system.

While state estimation occurs, the state of the system is reached in a time interval after T (i.e., $t > T$ to ∞); with this, the tracking enforcement of a reference can be achieved by the controller.

5. Simulation Results

The simulation validation is given in the following to underline the effectiveness and performance of the control strategy presented. The different parts of the self-sensing control method are illustrated in Figure 1. The nominal IPMSM parameters utilized in the simulations are presented in Table 1. Using Matlab/Simulink software, the simulation was performed. The engine is tested conforming to the industrial test trajectory [32] shown in Figure 2 which presents the trajectories of the chosen benchmark.
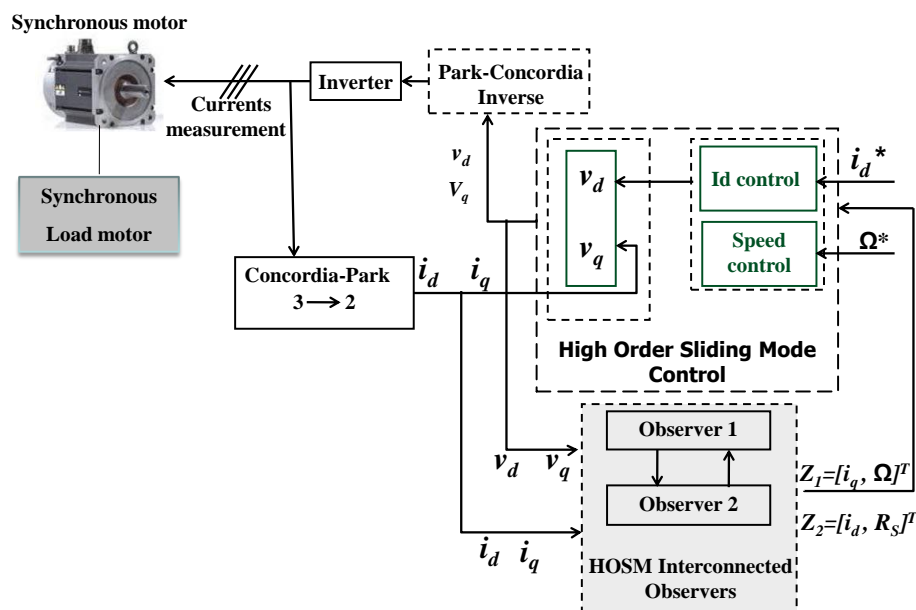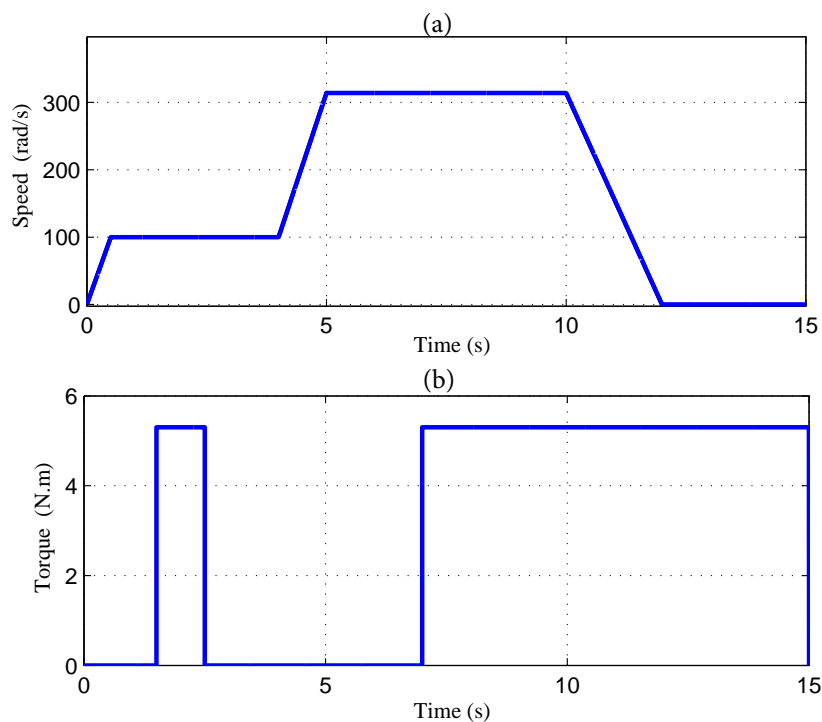

Figure 1. Observer–controller scheme.

Table 1. Internal permanent-magnet synchronous machine (IPMSM) specifications.

Rated power	2.3 kW	rated phase to phase voltage	380 V
Rated phase current	6 A	Torque	5.3 Nm
Speed	3000 rpm	ψ_f	0.341 Wb
Rated frequency	100 Hz	Windings connection	start connection
R_s	3.25 Ω	p	3
L_d	18 mH	L_q	34 mH
J	0.00417 kg·m^2	f_v	0.0034 kg·m^{2}s^{-1}

Figure 2. Industrial benchmark trajectory for: (**a**) speed; and (**b**) torque.

At the beginning, the motor is operated at zero speed without load torque to test the algorithms are developed in the critical observability area. Then the speed is increased to 100 rad/s and the load torque is applied for 1 s (from 1.5 s to 2.5 s). From the 4th s until the 6th s, the speed is increased up to 314 rad/s, and then it is kept constant for 10 s. By the 7th s, a load torque is applied. Stage two allows testing the observer during a high transition of speed as it enables testing its stability at a high-speed. By the final stage, both the motor's speed and the load torque reached zero; the former progressively dragged to zero (0) by the 13th s, while the later set to zero by the 15th s. In the case of nominal parameters, results depicted in Figures 3–6 confirm the efficiency of the implemented self-sensing control for IPMSM. The evolution of both estimated and observed speed schemes is presented in Figure 3a. The speed error caused by the perturbation is minimal; it tends rapidly to zero after the transients resulting from the application of the load torque (see Figure 3b). Figure 4 gives both position estimation and its measure. It is explicit that the observed position follows the real position exactly.
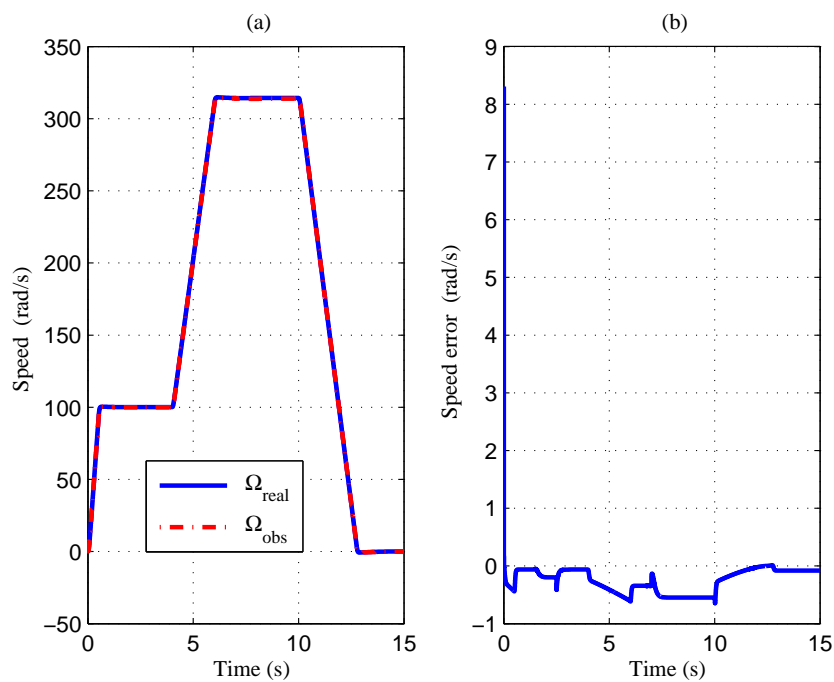
Figure 3. Tracking performance (nominal case): (**a**) observed and measured speeds; and (**b**) speed error.
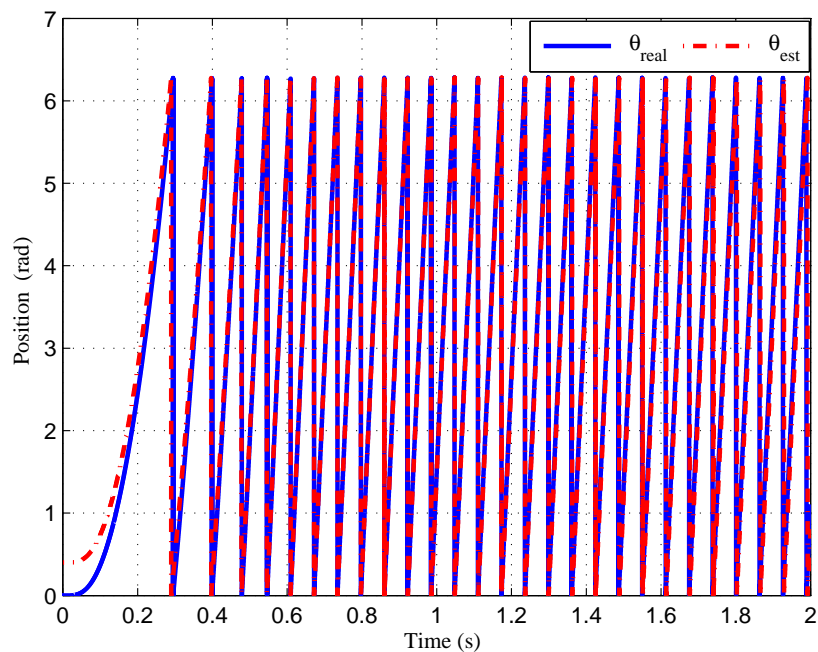

Figure 4. Observed and real position (nominal case).

In Figure 5, there is a good convergence of the estimated resistance with respect to its real value (see Figure 5b). It seems that the observer gives adequate results for these types of estimations. Figure 6 shows the input voltages and the *dq* currents. The effectiveness of the proposed strategy, especially in terms of chattering effect reduction, can be remarked on in this figure.
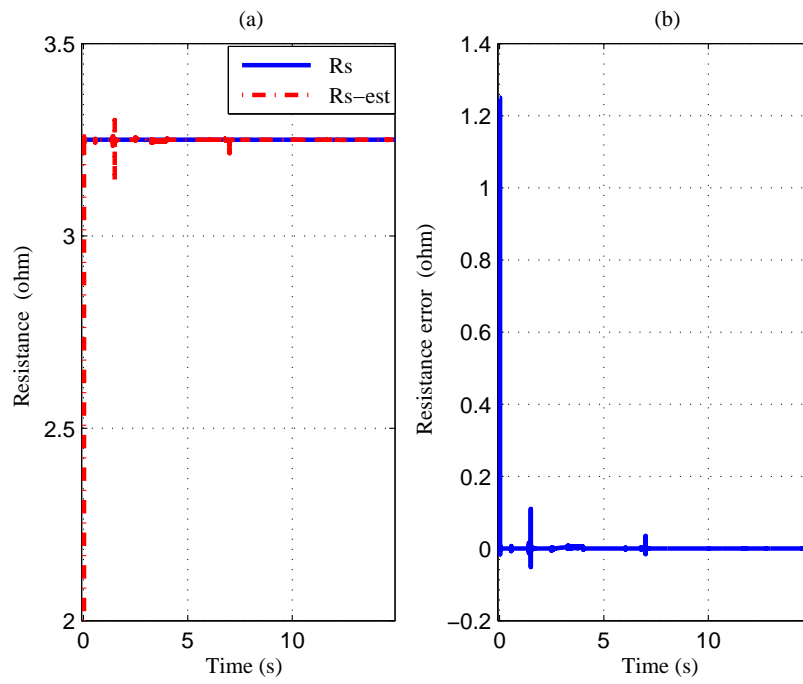
Figure 5. Estimation performance (nominal case): (**a**) estimated and real resistance; and (**b**) estimation error.
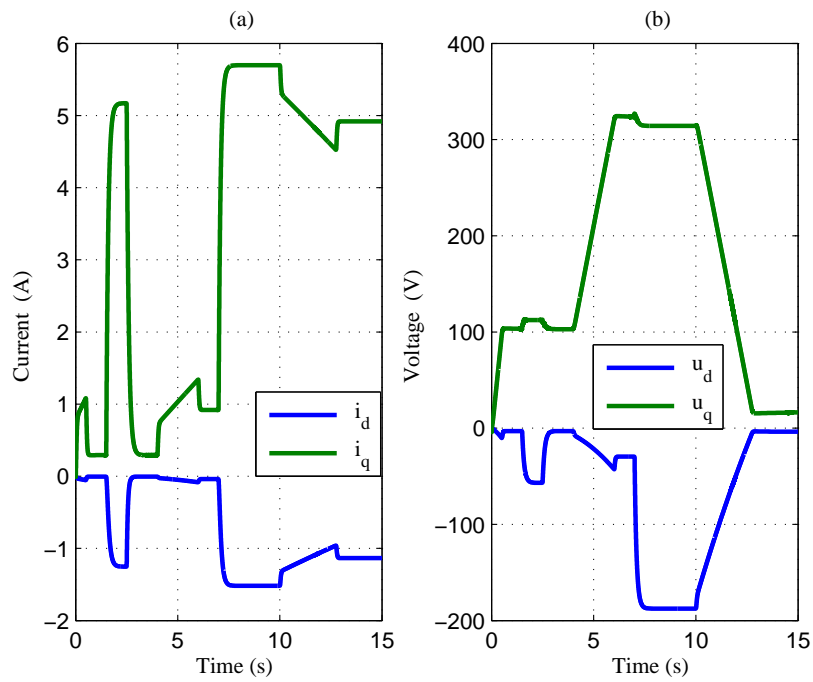
Figure 6. Tracking performance (nominal case): (**a**) dq currents; and (**b**) dq voltages.

The influence of parameter variations was examined to show the robustness of the self-sensing control scheme. The Voluntary add of the variation of parameters in the controller observer scheme was introduced. Figures 7 and 8 and Figures 9 and 10 present the response of the system with, respectively, +30% and −30% of the variation in stator resistance. The effectiveness of the resistance estimator is noticed mutually at the different speed ranges.
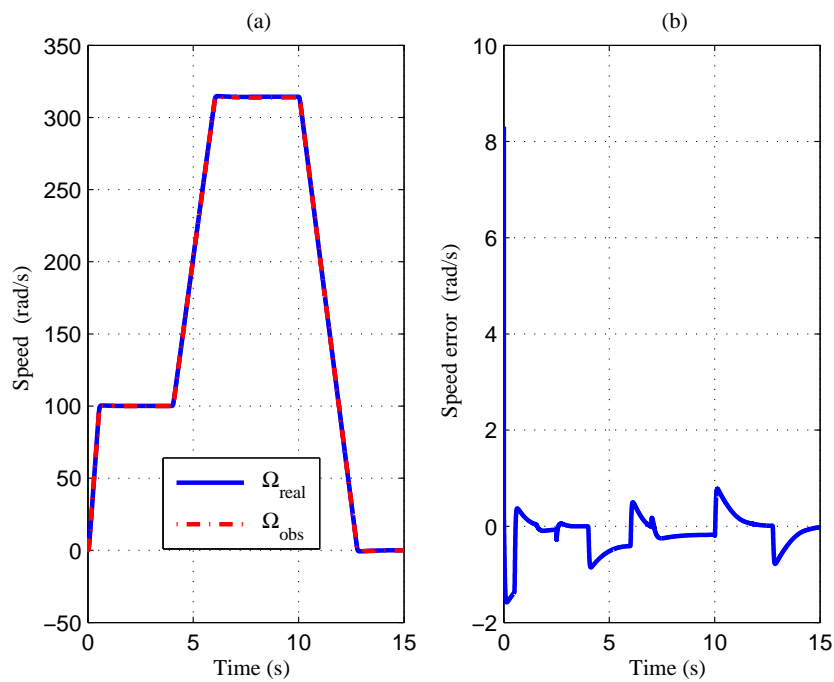
Figure 7. Robustness w.r.t. −30% R_s: (**a**) observed and measured speeds; and (**b**) speed error.
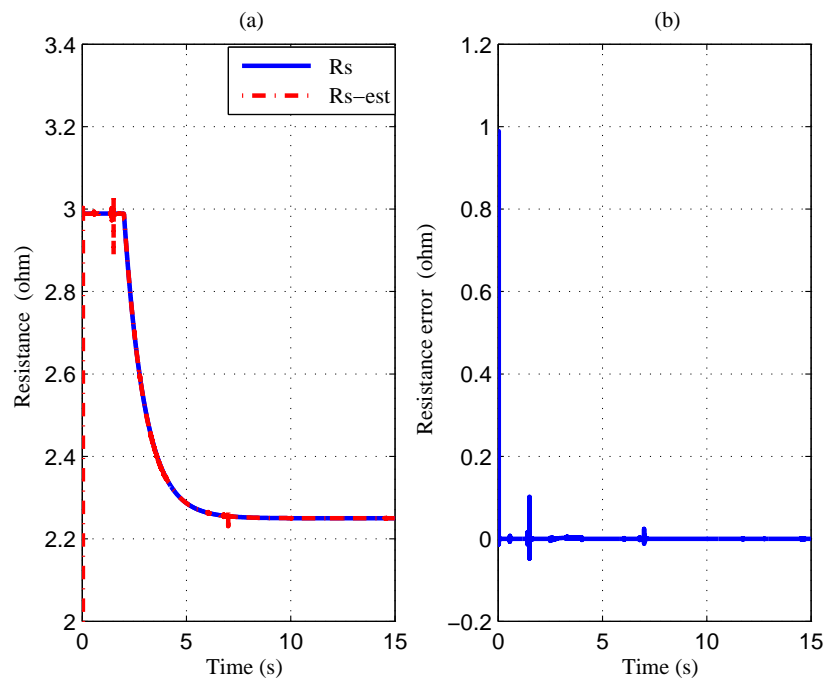
Figure 8. Robustness w.r.t. −30% R_s: (**a**) estimated and real resistance; and (**b**) estimation error.
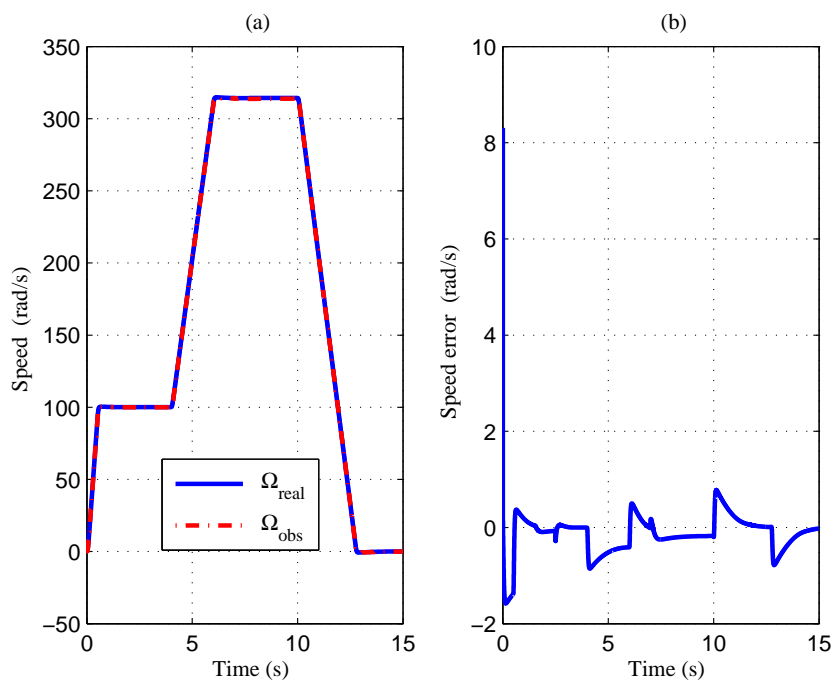
Figure 9. Robustness w.r.t. +30% R_s: (**a**) observed and measured speeds; and (**b**) speed error.
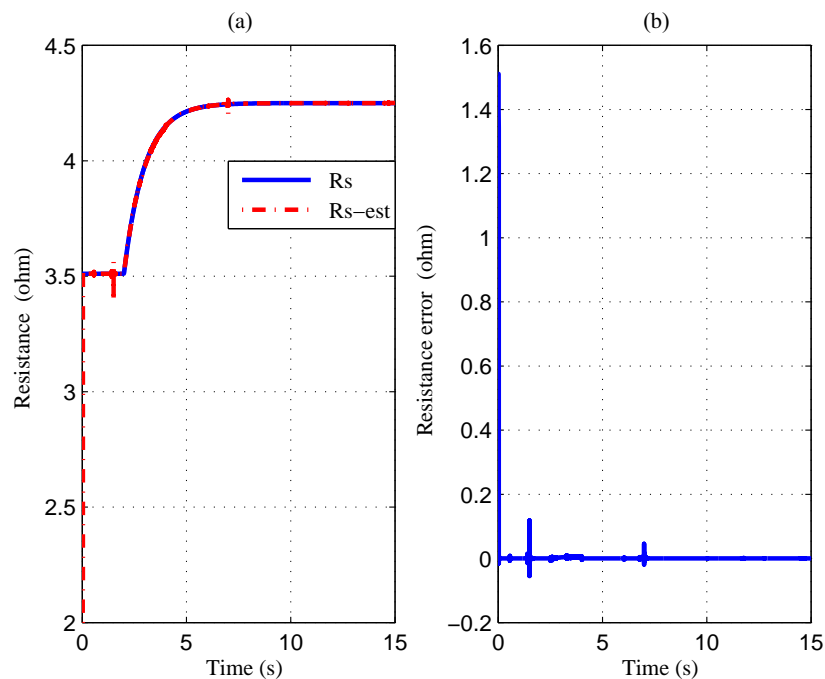
Figure 10. Robustness w.r.t. +30% R_s: (**a**) estimated and real resistance; and (**b**) estimation error.

The suggested resistance estimator makes possible the mitigation of the unwanted effects of stator resistance variations. The latest test is to introduce a fluctuation of $\pm 20\%$ in the stator inductances. The system's response under the control observer action is shown in Figures 11 and 12, where it can be seen that the variations in the stator inductance do not affect the system. The robustness and efficiency of the self-sensing control suggested, with variations of parameters and load torque, are apparent. The controller's gains are selected as follows: $\lambda_{1,1} = 1500$, $\lambda_{1,2} = 400$, $\lambda_{2,1} = 200$.

The observer parameter values: $\alpha_{11} = 900$, $\alpha_{12} = 1500$, $\alpha_{21} = 850$, $\alpha_{22} = 700$, $K_\theta = 16$.
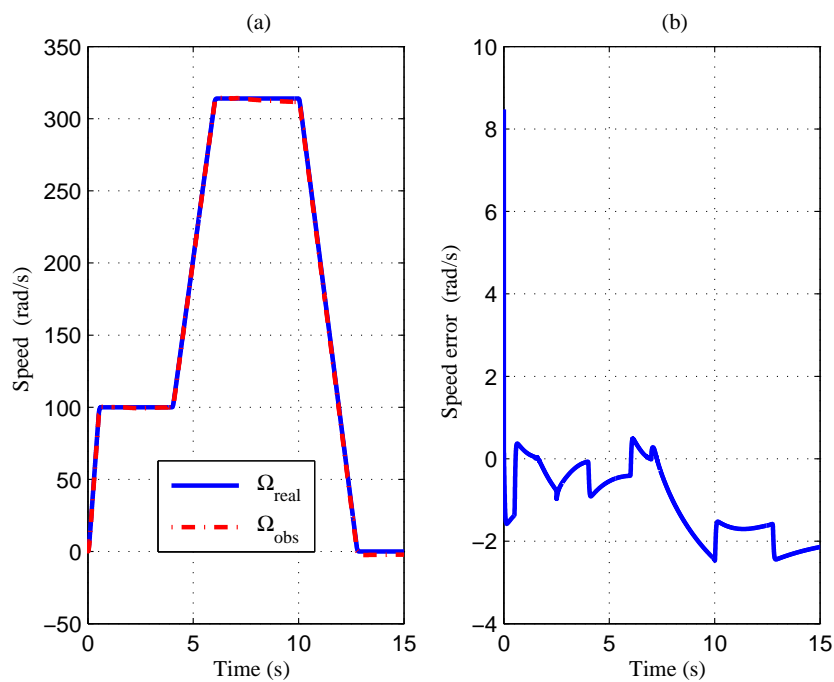
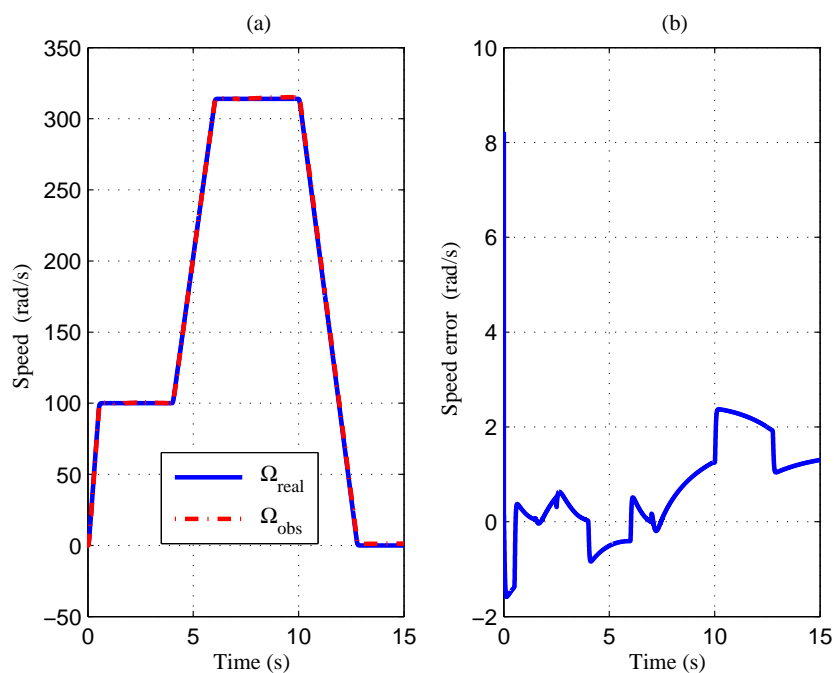**Figure 11.** Robustness w.r.t. +20% L_d, L_q: (**a**) observed and measured speeds; and (**b**) speed error.

Figure 12. Robustness w.r.t. −20% L_d, L_q: (**a**) observed and measured speeds; and (**b**) speed error.

6. Conclusions

In this work a self-sensing control of a permanent magnet magnet synchronous machine is introduced. The described strategy is based on a higher order sliding mode controller and observer. The proposed controller is a good combination between the backstepping and higher order sliding mode strategies. Therefore, the gains of sliding mode are reduced compared to the classical one. With the proposed controller the finite time convergence of the tracking errors is obtained and the chattering effect is attenuated as can be seen in the control output. Moreover, this controller allowed

the rejection of the unmatched perturbations (parameter uncertainties in this case) and the rejection of the external perturbations. On the other hand, the super twisting algorithm is generalised for multi-input–multi-output systems by combining it with the interconnected observer strategy. The new observer is applied to estimate the rotor position, rotor speed and the stator resistance. The finite-time convergence of the estimated states to the measured one is proven. As the finite-time convergence of the controller and the observer are proven separately, the stability of the proposed observer–controller scheme can be achieved according to the separation principle. The proposed controller and observer are implemented in simulation to realise the self-sensing control of IPMSM. The obtained results show clearly the effectiveness of the developed strategy. The robustness tests made to show the efficiency of the proposed one, despite the presence of electrical parameter uncertainties, show its good ability. Our future work will be on how to deal with the problem of saturation of machine inductance and, after that, to generalise the proposed strategy to all electrical machines.

References

1. Athavale, A.; Sasaki, K.; Gagas, B.S.; Kato, T.; Lorenz, R.D. Variable Flux Permanent Magnet Synchronous Machine (VF-PMSM) Design Methodologies to Meet Electric Vehicle Traction Requirements with Reduced Losses. *IEEE Trans. Ind. Appl.* **2017**, *53*, 4318–4326. [CrossRef]
2. Liu, F.; Xu, L.; Li, Y.; Kang, Y.; Wu, Z. Permanent magnet synchronous machine starter/generators based high-voltage DC parallel electric power system for the more electric aircraft. *J. Eng.* **2018**, *2018*, 565–569. [CrossRef]
3. Liu, J.; Zhu, Z. Improved Sensorless Control of Permanent-Magnet Synchronous Machine Based on Third-Harmonic Back EMF. *IEEE Trans. Ind. Appl.* **2014**, *50*, 1861–1870. [CrossRef]
4. Divandari, M.; Rezaie, B.; Noei, A.R. Speed control of switched reluctance motor via fuzzy fast terminal sliding-mode control. *Comput. Electr. Eng.* **2019**, *80*, 106472. [CrossRef]
5. Zhan, H.; Zhu, Z.Q.; Odavic, M. Nonparametric Sensorless Drive Method for Open-Winding PMSM Based on Zero-Sequence Back EMF With Circulating Current Suppression. *IEEE Trans. Power Electron.* **2017**, *32*, 3808–3817. [CrossRef]
6. Genduso, F.; Miceli, R.; Rando, C.; Galluzzo, G.R. Back EMF Sensorless-Control Algorithm for High-Dynamic Performance PMSM. *IEEE Trans. Ind. Electron.* **2010**, *57*, 2092–2100. [CrossRef]
7. Bolognani, S.; Ortombina, L.; Tinazzi, F.; Zigliotto, M. Model sensitivity of fundamental-frequency-based position estimators for sensorless pm and reluctance synchronous motor drives. *IEEE Trans. Ind. Electron.* **2018**, *65*, 77–85. [CrossRef]
8. Dian, R.; Xu, W.; Zhu, J.; Hu, D.; Liu, Y. An Improved Speed Sensorless Control Strategy for Linear Induction Machines Based on Extended State Observer for Linear Metro Drives. *IEEE Trans. Veh. Technol.* **2018**, *67*, 9198–9210. [CrossRef]
9. Hamida, M.A.; De Leon, J.; Glumineau, A.; Boisliveau, R. An Adaptive Interconnected Observer for Sensorless Control of PM Synchronous Motors with Online Parameter Identification. *IEEE Trans. Ind. Electron.* **2013**, *60*, 739–748. [CrossRef]
10. Taherzaheh, M.; Hamida, M.; Ghanes, M.; Koteich, M. A New Torque Observation Technique for a PMSM Considering Unknown magnetic Conditions. *IEEE Trans. Ind. Electron.* **2020**, 1. [CrossRef]

11. Saïd, S.H.; M'Sahli, F.; Mimouni, M.; Farza, M. Adaptive high gain observer based output feedback predictive controller for induction motors. *Comput. Electr. Eng.* **2013**, *39*, 151–163. [CrossRef]

12. Kadrine, A.; Tir, Z.; Malik, O.P.; Hamida, M.A.; Reatti, A.; Houari, A. Adaptive non-linear high gain observer based sensorless speed estimation of an induction motor. *J. Frankl. Inst.* **2020**. [CrossRef]

13. Senanayaka, J.S.L.; Karimi, H.R.; Robbersmyr, K.G. Sensorless small wind turbine with a sliding-mode observer for water heating applications. In Proceedings of the IECON 2015-41st Annual Conference of the IEEE Industrial Electronics Society, Yokohama, Japan, 9–12 November 2015; pp. 000863–000868.

14. Shtessel, Y.; Taleb, M.; Plestan, F. A novel adaptive-gain supertwisting sliding mode controller: Methodology and application. *Automatica* **2012**, *48*, 759–769. [CrossRef]

15. Davila, J.; Fridman, L.; Levant, A. Second-order sliding-mode observer for mechanical systems. *IEEE Trans. Autom. Control* **2005**, *50*, 1785–1789. [CrossRef]

16. Zerdali, E.; Barut, M. The Comparisons of Optimized Extended Kalman Filters for Speed-Sensorless Control of Induction Motors. *IEEE Trans. Ind. Electron.* **2017**, *64*, 4340–4351. [CrossRef]

17. Cheng, H.; Chen, H.; Xu, S.; Yang, S. Four-quadrant sensorless control in switched reluctance machine drive using pulse injection based on special flux linkage curves. *IET Electr. Power Appl.* **2017**, *11*, 1566–1574. [CrossRef]

18. Hamida, M.A.; Glumineau, A.; De Leon, J. Robust Integral Backstepping Control for Sensorless IPM Synchronous Motor Controller. *J. Frankl. Inst.* **2012**, *349*, 1734–1757. [CrossRef]

19. Wang, G.; Yang, L.; Zhang, G.; Zhang, X.; Xu, D. Comparative Investigation of Pseudorandom High-Frequency Signal Injection Schemes for Sensorless IPMSM Drives. *IEEE Trans. Power Electron.* **2017**, *32*, 2123–2132. [CrossRef]

20. Kwon, Y.; Sul, S. Reduction of Injection Voltage in Signal Injection Sensorless Drives Using a Capacitor-Integrated Inverter. *IEEE Trans. Power Electron.* **2017**, *32*, 6261–6274. [CrossRef]

21. Lu, K.; Lei, X.; Blaabjerg, F. Artificial Inductance Concept to Compensate Nonlinear Inductance Effects in the Back EMF-Based Sensorless Control Method for PMSM. *IEEE Trans. Energy Convers.* **2013**, *28*, 593–600. [CrossRef]

22. Qiao, Z.; Shi, T.; Wang, Y.; Yan, Y.; Xia, C.; He, X. New Sliding-Mode Observer for Position Sensorless Control of Permanent-Magnet Synchronous Motor. *IEEE Trans. Ind. Electron.* **2013**, *60*, 710–719. [CrossRef]

23. Hamida, M.; Leon, J.D.; Glumineau, A. High-order sliding mode observers and integral backstepping sensorless control of IPMS motor. *Int. J. Control* **2014**, *87*, 2176–2193. [CrossRef]

24. Mystkowski, A. Lyapunov sliding-mode observers with application for active magnetic bearing operated with zero-bias flux. *J. Dyn. Syst. Meas. Control* **2019**, *141*, 041006. [CrossRef]

25. Liang, D.; Li, J.; Qu, R.; Kong, W. Adaptive Second-Order Sliding-Mode Observer for PMSM Sensorless Control Considering VSI Nonlinearity. *IEEE Trans. Power Electron.* **2018**, *33*, 8994–9004. [CrossRef]

26. Liang, D.; Li, J.; Qu, R. Sensorless Control of Permanent Magnet Synchronous Machine Based on Second-Order Sliding-Mode Observer With Online Resistance Estimation. *IEEE Trans. Ind. Appl.* **2017**, *53*, 3672–3682. [CrossRef]

27. Pillay, P.; Krishnan, R. Modeling, simulation, and analysis of permanent-magnet motor drives. II. The brushless DC motor drive. *IEEE Trans. Ind. Appl.* **1989**, *25*, 274–279. [CrossRef]

28. Estrada, A.; Fridman, L.; Iriarte, R. Combined backstepping and HOSM control design for a class of nonlinear MIMO systems. *Int. J. Robust Nonlinear Control* **2017**, *27*, 566–581. [CrossRef]

29. Gonzalez-Gutierrez, C.A.; Rodriguez-Resendiz, J.; Mota-Valtierra, G.; Rivas-Araiza, E.A.; Mendiola-Santibanez, J.D.; Luna-Rubio, R. A PC-based architecture for parameter analysis of vector-controlled induction motor drive. *Comput. Electr. Eng.* **2011**, *37*, 858–868. [CrossRef]

30. Inoue, T.; Inoue, Y.; Morimoto, S.; Sanada, M. Mathematical Model for MTPA Control of Permanent-Magnet Synchronous Motor in Stator Flux Linkage Synchronous Frame. *IEEE Trans. Ind. Appl.* **2015**, *51*, 3620–3628. [CrossRef]

31. Filippov, A.F. *Differential Equations with Discontinuous Right-Hand Sides*; Kluwer: Dortrecht, The Netherlands, 1998.
32. Hamida, M.; de Leon, J.; Glumineau, A. Experimental sensorless control for IPMSM by using integral backstepping strategy and adaptive high gain observer. *Control Eng. Pract.* **2017**, *59*, 64–76. [CrossRef]

Sample Availability: Samples of the compounds . . . . . . are available from the authors.